Acta Pharmaceutica Sinica B 2024;14(3):1441−1456

Chinese Pharmaceutical Association
Institute of Materia Medica, Chinese Academy of Medical Sciences

Acta Pharmaceutica Sinica B

www.elsevier.com/locate/apsb
www.sciencedirect.com

ORIGINAL ARTICLE

Genome editing of *PAR2* through targeted delivery of CRISPR-Cas9 system for alleviating acute lung inflammation *via* ERK/NLRP3/IL-1β and NO/iNOS signalling

Xin Zhuo, Yue Wu, Xiujuan Fu, Jianbin Li, Yuxin Xiang, Xiaoyu Liang, Canquan Mao, Yuhong Jiang*

Sichuan Engineering Research Center for Biomimetic Synthesis of Natural Drugs, School of Life Science and Engineering, Southwest Jiaotong University, Chengdu 610031, China

Received 16 April 2023; received in revised form 24 June 2023; accepted 26 June 2023

KEY WORDS

Protease-activated receptor 2 (PAR2);
CRISPR-Cas9;
Gene editing;
Inflammation;
Acute lung inflammation;
NLRP3;
Nanoparticles;
Drug delivery

Abstract Excessive and uncontrollable inflammatory responses in alveoli can dramatically exacerbate pulmonary disease progressions through vigorous cytokine releases, immune cell infiltration and protease-driven tissue damages. It is an urgent need to explore potential drug strategies for mitigating lung inflammation. Protease-activated receptor 2 (PAR2) as a vital molecular target principally participates in various inflammatory diseases *via* intracellular signal transduction. However, it has been rarely reported about the role of PAR2 in lung inflammation. This study applied CRISPR-Cas9 system encoding Cas9 and sgRNA (*pCas9-PAR2*) for *PAR2* knockout and fabricated an anionic human serum albumin-based nanoparticles to deliver *pCas9-PAR2* with superior inflammation-targeting efficiency and stability (TAP/*pCas9-PAR2*). TAP/*pCas9-PAR2* robustly facilitated *pCas9-PAR2* to enter and transfect inflammatory cells, eliciting precise gene editing of *PAR2 in vitro* and *in vivo*. Importantly, *PAR2* deficiency by TAP/*pCas9-PAR2* effectively and safely promoted macrophage polarization, suppressed pro-inflammatory cytokine releases and alleviated acute lung inflammation, uncovering a novel value of PAR2. It also revealed that PAR2-mediated pulmonary inflammation prevented by TAP/*pCas9-PAR2* was mainly dependent on ERK-mediated NLRP3/IL-1β and NO/iNOS signalling. Therefore, this work indicated PAR2 as a novel target for lung inflammation and provided a potential nanodrug strategy for *PAR2* deficiency in treating inflammatory diseases.

*Corresponding author.
E-mail addresses: yuh.jiang@foxmail.com, yuhong.jiang@swjtu.edu.cn (Yuhong Jiang).

Peer review under the responsibility of Chinese Pharmaceutical Association and Institute of Materia Medica, Chinese Academy of Medical Sciences.

https://doi.org/10.1016/j.apsb.2023.08.013

1. Introduction

Inflammation as a naïve defence response of the body can eradicate pathogens to the host organism[1,2]. However, sustained and excessive inflammatory responses provoke a range of adverse effects, including tissue damage, edema and cytokine storm. Acute lung inflammation (ALI) is critically initiated by extensive inflammatory responses in the lung as a core respiratory organ, largely impairing respiratory system[3]. Emerging evidence has revealed that ALI is usually associated with potent proinflammatory cytokine release, protease and immune cell accumulation, and edema in alveoli, exhibiting the mortality rate of 35%−45%[3,4]. Importantly, coronavirus disease 2019 (COVID-19) as a novel type of pneumonia possesses elevated pulmonary inflammation with aggravation of cytokine storm[5,6]. The blockade of lung inflammatory responses and massive proinflammatory cytokines may dramatically mitigate the severe exacerbation of COVID-19. Indeed, it is an emergent need for probing drug targets and strategies in treating pulmonary inflammatory diseases.

Protease-activated receptor 2 (PAR2) belonging to G protein-coupled receptors (GPCRs) actively participates in various inflammatory diseases, such as paw edema, irritable bowel syndrome[7,8]. PAR2 can be cleaved and activated by certain proteases to modulate downstream inflammatory signal transduction, while ALI can evoke abundant secretions of proteases[4,9], suggesting the possible role of PAR2 in lung inflammation. Additionally, PAR2 activated by proteases or synthetic ligands can powerfully initiate plentiful proinflammatory cytokine releases in flamed tissues[10] which are also involved in lung inflammatory diseases. However, there is rare investigations on the relationship between PAR2 and pulmonary inflammation, despite targeting PAR2 as a potential and extraordinary therapeutical strategy for other inflammatory diseases.

To probe the participation of PAR2 in pulmonary inflammatory diseases, CRISPR-Cas9 technology can be utilized to evoke specific gene editing for accurate PAR2 inhibition. As a novel and powerful genome-editing tool, the plasmid-based CRISPR-Cas9 all-in-one system that encodes Cas9 and sgRNA targeting specific gene has been widely used for gene knockout in disease treatment[11]. Due to the obstacles of large size, negative charge and nuclease degradation, plasmid itself cannot trigger effective and safe gene editing, while various approaches including nanoparticles have been applied for CRISPR-Cas9 plasmid delivery[12]. Nanoparticle delivery system for CRISPR-Cas9 mainly focuses on cationic lipid nanoparticles, such as liposome, cationic polymers and lipid-based nanoparticles, which can condense plasmid and robustly improve gene editing efficiency of CRISPR-Cas9 for preventing disease progression[13−15]. However, such cationic nanoparticles usually exhibit high systemic toxicity that largely restricted effectiveness and safety of CRISPR-Cas9[16]. Human serum albumin (HSA) as natural biomaterials with excellent biocompatibility can be modified to encapsulate gene drugs for enhanced cell uptake and transfection efficacy *in vitro* and *in vivo* with low toxicity, suggesting that it is a potential alternative candidate for CRISPR-Cas9 delivery[17,18].

In this work, we developed an anionic albumin-based nanoparticle to encapsulate CRISPR-Cas9 plasmid encoding Cas9 and *PAR2* sgRNA (*pCas9-PAR2*). Moreover, it has reported that elevated levels of collagen accumulated in inflamed sites and a collagen-binding peptide (CBP) can precisely target to inflammatory tissues *via* high collagen affinity[19]. Therefore, CBP was conjugated to the surface of HSA nanoparticles to enhance inflammation-targeting efficiency, consequently constructing inflammation-targeted albumin-PEI nanoparticles that encapsulated *pCas9-PAR2* (TAP/*pCas9-PAR2*). Although it has been considered that cationic nanoparticles but not anionic materials can preferably improve cell uptake and transfection of genes *via* interacting with negative charge of cell membrane[20], the anionic TAP/*pCas9-PAR2* successfully delivered CRISPR-Cas9 into cells with high cell transfection efficiency, and subsequently provoke gene editing of *PAR2* in inflammatory cells. *PAR2* deficiency initiated M1 to M2 macrophage polarization and prevented PAR2-specific or unspecific paw edema. Furthermore, TAP/*pCas9-PAR2* safely and effectively targeted to inflamed lungs and evoked *PAR2* knockout *in vivo* to eliminate PAR2-induced ALI, revealing the new role of *PAR2* in lung inflammation. More importantly, we uncovered its underlying mechanism of this nanodrug, in which *PAR2* deficiency by TAP/*pCas9-PAR2* alleviated PAR2-mediated lung inflammation *via* ERK/NLRP3/IL-1β and NO/iNOS signalling.

2. Materials and methods

2.1. Materials and cell culture

Human serum albumin (HSA) was purchased from Sigma (Cas No. 70024-90-7, St. Louis, MO, USA), while poly-(ethylene imine) (PEI 10K), glutaraldehyde, λ-carrageenan were obtained from Adamas (Cas No. 9002-98-6, 111-30-8, 9064-57-7, Shanghai, China). 2-Furoyl-LIGRL-NH_2 (2f-LIGRL-NH_2, 2f, 98%) and collagen-binding peptide (CBP, LRELHLNNNC, 98%) were custom-made by Apeptides (Shanghai, China). The primary antibodies against total/phospho-ERK were purchased from Cell Signaling Technology (Cat No. 4695S, 4370S, Boston, MA, USA). The primary antibodies against PAR2, NLRP3, iNOS and GAPDH were obtained from Abcam (Cat No. ab180953, ab263899, ab178945, ab181602, Cambridge, MA, USA). The secondary antibodies HRP-conjugated anti-rabbit IgG was obtained from Invitrogen (Cat No. 31460, Carlsbad, CA, USA). The e*SpCas9*-2A-Puro (PX459) V2.0 plasmid encoding Cas9 and human or murine *PAR2* sgRNA, and the e*SpCas9*-2A-GFP (PX458) plasmid with Cas9, GFP and *PAR2* sgRNA were constructed by GenScript (Nanjing, China).

The human non-small cell lung cancer A549 cell line and mouse leukemia cells of monocyte-macrophage RAW264.7 cell line were obtained from Sichuan University. Cells were cultured in DMEM medium (Cat No. 10-013-CVR, Corning, New York, NY, USA), supplemented with 10% fetal bovine serum (Gibco, Carlsbad, CA, USA) and 100 U/mL penicillin/streptomycin at 37 °C in a humidified incubator containing 5% CO_2.

2.2. Preparation of nanoparticles

HSA nanoparticles encapsuled CRISPR-Cas9 encoding *PAR2* gRNA and Cas9 (*pCas9-PAR2*) were constructed by a modified desolvation technique as described previously[17,18,21]. Briefly, HSA and PEI were dissolved in ddH_2O (pH 8.0), respectively. HSA, PEI and *pCas-PAR2* were vortexed for 20 s and then incubated for 20 min. Subsequently, 2 mL ethanol was added dropwise to the mixture under stirring at 500 rpm (Cat No. 0005019825, Ika, Germany) at room temperature for 30 min. The mixture was then crosslinked with 100 μL 2.5% glutaraldehyde under stirring for 30 min. Finally, collagen-binding peptide (CBP) was added and stirred at 220 rpm at 4 °C overnight for forming CBP-grafted HSA-PEI-*pCas9-PAR2* nanoparticles (TAP/*pCas9-PAR2*). For preparing albumin-PEI nanoparticles without CBP that encapsulated *pCas9-PAR2* (AP/*pCas9-PAR2*), HSA nanoparticles were crosslinked with 2.5% glutaraldehyde under stirring at 220 rpm at 4 °C overnight. All nanoparticles were washed and redispersed with ddH_2O through repeated ultracentrifugation for separating unencapsulated plasmid.

2.3. Physicochemical characterization of nanoparticles

The size, PDI and Zeta potential of nanoparticles were measured by the dynamic light scattering (DLS) technique (ZEN3600, Malvern, UK). For morphology, nanoparticles were observed by transmission electron microscope (TEM, JEM-2100F, Tokyo, Japan). To investigate their stability, the size and PDI of nanoparticles were measured over 30 days. The fluorescent dye SYBR Green was used to measure plasmid concentration. Free plasmids with various concentrations were used to establish a standard curve, and the unencapsulated *pCas9-PAR2* was collected after ultracentrifugation. All plasmids were incubated with SYBR Green for 10 min, while the unencapsulated plasmid concentration was evaluated by detecting the fluorescence of SYBR Green-conjugated plasmids. The weight of encapsulated plasmid was subtraction of unencapsulated plasmid from total plasmid. The encapsulation efficiency and drug loading capacity were calculated as in Eqs. (1) and (2):

$$\text{Encapsulation efficiency } (\%) = \frac{\text{Weight of encapsulated plasmid}}{\text{Weight of total plasmid}} \times 100 \quad (1)$$

$$\text{Drug loading capacity}(\%) = \frac{\text{Weight of encapsulated plasmid}}{\text{Weight of NPs}} \times 100 \quad (2)$$

2.4. In vitro cellular uptake

Cy5-DNA as a fluorescent DNA substitution for *pCas9-PAR2* to evaluate cell uptake efficiency of nanoparticles. Cells were seeded at 24 well plates overnight and were treated with Cy5-DNA and different nanoparticles (equal to 1 μg Cy5-DNA) for 1 h. Cells were then washed three times with PBS, and cellular uptake efficiency was determined by flow cytometry (AccuriTM C6 flow cytometer, Becton Dickinson, NJ, USA).

2.5. In vitro cellular transfection

GFP-tagged *pCas9-PAR2* (GFP-*pCas9-PAR2*) was used for detection of cell transfection. Cells were seeded in 24 well plates overnight and treated with GFP-*pCas9-PAR2* and nanoparticles (equal to 1 μg GFP-*pCas9-PAR2*) for 4 h. Cells were then washed with PBS and medium was replaced with fresh medium for further 44 h. After that, cells were washed with PBS three times and determined by flow cytometry (Becton Dickinson). Alternatively, after transfection, cells were stained with DAPI and observed by confocal microscopy (FV-OSR, Olympus, Tokyo, Japan).

2.6. In vitro cytotoxicity

Cells were seeded at a 96 well plate overnight. Cells were then treated with nanoparticles for 4 h and medium was replaced with fresh medium for further 44 h. Alternatively, cells were treated with nanoparticles for 48 h experiment. After that, cells were incubated with CCK8 (Cat No. K101826433EF5E, APExBIO, Houston, TX, USA) and measured at 450 nm.

2.7. DNase protection assay

pCas9-PAR2 and nanoparticles were incubated with DNase (Cat No. 1078S, TaKaRa, Kyoto, Japan) for 30 min at 37 °C, and then added with 1M EDTA to stop the reaction. Cells were incubated with DNase-treated and untreated *pCas9-PAR2* and nanoparticles for 4 h. Cells were then thoroughly washed three times with PBS and incubated with a fresh medium for another 44 h. Fluorescence images were observed by fluorescence microscopy.

2.8. T7 endonuclease I (T7EI) assay and sanger sequencing analysis

Cells were seeded at 24 well plates overnight and treated with different nanoparticles for 48 h. Genomic DNA was extracted and amplified according to the manufacturer's instructions. PCR products diluted in reaction buffer were annealed in a thermocycler using the following conditions (95 °C for 5 min, −2 °C/s to 85 °C and −0.1 °C/s to 25 °C, and then cooling down to 4 °C). After that, T7EI (Cat No. 017E229GA, Vazyme, Nanjing, China) was added and incubated at 37 °C for 15 min. The cleavage reaction was stopped by 0.25 mol/L EDTA. The fragmented DNA were subjected to electrophoresis and was analyzed by ImageJ. The cleavage percentage was calculated by Eq. (3):

$$\text{Cleavage } (\%) = (1-(1-\text{Fraction cleaved})^{1/2}) \times 100 \quad (3)$$

The primers are listed in Supporting Information Table S1. PCR products were also subcloned by a TA/Blunt-Zero cloning kit (Cat No. 017E2210IA, Vazyme), and were randomly picked for sanger sequencing by Tsingke Biotechnology Co., Ltd.

2.9. Real-time quantitative PCR (qRT-PCR)

Cells were seeded at 24 well plates overnight and were incubated with different nanoparticles containing 2 μg *pCas9-PAR2* for 30 h. 25 μmol/L 2f-LIGRL-NH_2 and 1 μg/mL LPS was then added for further 18 h. RNA was isolated using TRIzol™ Reagent (Cat No.

15596026, Invitrogen) according to manufacturer's instructions. One microgram of isolated RNA was reverse transcribed using HiScript III 1st Strand cDNA Synthesis Kit (Cat No. 7F581J1, Vazyme) for cDNA synthesis. qRT-PCR analysis was performed using ChamQ Universal SYBR qPCR Master Mix (Cat No. 027E1280LA, Vazyme) with suitable primers. The primers used are listed in Table S1.

2.10. Western blotting

Cells were seeded at 12 well plates overnight, and were then incubated with different nanoparticles containing 2 μg *pCas9-PAR2* for 30 h. 25 μmol/L 2f-LIGRL-NH_2 and 1 μg/mL LPS was then added for 18 h. Cells were lysed with RIPA buffer containing PMSF. Protein samples were separated using SDS-PAGE and transferred to the NC membrane. After blocked, membrane was incubated overnight with primary antibodies and HRP-conjugated goat anti-rabbit IgG secondary antibody was added for 2 h. Bands were visualized using a BeyoECL Moon (Cat No. P0018AS, Beyotime, Shanghai, China), and the software ImageJ was applied for quantitative analysis.

2.11. PAR2 gene and protein expression detection

Cells were seeded at 24 well plates overnight and were then treated with different nanoparticles for 48 h. For gene expression, total RNA of cells was isolated and then *PAR2* gene expression was detected by RT-PCR. For cell surface expression of PAR2, cells were incubated with the primary antibody against PAR2 in PBS for 1 h and were then incubated with Cy3-conjugated affinipure goat anti-rabbit IgG followed by fluorescence detection using flow cytometry analysis (Becton Dickinson). For PAR2 protein expression, lung tissues were lysed and detected by Western blotting technique after drug treatments.

2.12. PAR2 agonist-induced and λ-carrageenan-induced paw edema

All experimental procedures were executed according to the protocols approved by Southwest Jiaotong University Animal Care and Use Committee. Before administration, the thickness and width of left hind paw of each male mouse (4 weeks) was measured as an internal control. Mice were intravenously injected with *pCas9-PAR2*, AP/*pCas9-PAR2* or TAP/*pCas9-PAR2* containing 10 μg *pCas9-PAR2*. After 24 h, the left hind paw pad was injected with 2-furoyl-LIGRL-NH_2 (2f, 350 μg/paw) for PAR2-specific paw edema, λ-carrageenan for non-specific paw edema or saline control. Paw measurements were measured within different time points post injection. The paw was cut off and stained with hematoxylin and eosin (H&E) for histopathological analysis. The paw swelling degree was calculated as thickness × width normalized to maximal swelling (100%).

2.13. Establishment of acute lung inflammation (ALI) model

For acute lung inflammation model, mice (C57BL/6, male, 6 weeks) were randomly divided into six groups. Mice were anesthetized and nasally administrated with saline, LPS or LPS+2f (LPS: 50 μg, 2f: 250 μg). After 2 h, mice were intravenously injected with saline, *pCas9-PAR2*, AP/*pCas9-PAR2* or TAP/*pCas9-PAR2* containing 10 μg *pCas9-PAR2*. After 48 h, mice underwent bronchus-alveolus lavage with saline, and the supernatant of bronchoalveolar lavage fluid (BALF) was collected and stored at −80 °C. The precipitated cells were resuspended with PBS, and the total cell numbers of BLAF were counted on a hemocytometer and observed with Wright−Giemsa staining. The protein concentrations in the BALF were determined by BCA kit. Alternatively, lungs were fixed with 4% formaldehyde for histopathological analysis, or were collected for detecting protein levels by Western blotting.

2.14. ELISA

BALF was collected from ALI model and the concentrations of inflammatory factors (IL-6, TNF-α and IL-1β) in BALF were quantified by ELISA Kit (Cat No. 1210602, 1217202, 1210122, DAKEWE, Shenzhen, China) according to the manufacturer's instructions.

2.15. Pharmacokinetic studies

Healthy mice were intravenously injected with Cy5-DNA and Cy5-DNA-loaded nanoparticles. The blood from orbit was collected at 0, 1, 5, 10, 30 min, 1, 2, 3, 6, and 24 h after administration. Free Cy5-DNA with different concentrations were used to prepare a Cy5 standard curve (Supporting Information Table S2). The blood was diluted, and fluorescence was detected (Ex = 640 nm, Em = 670 nm). Pharmacokinetics parameters were calculated to fit a two-compartment model by DAS software.

2.16. In vivo biodistribution and targeting efficacy in inflamed lungs

Acute lung inflammation model was constructed as described above. Mice were intravenously injected with 10 μg Cy5-DNA and Cy5-DNA-loaded nanoparticles. Mice were sacrificed and organs (heart, liver, spleen, lung, and kidney) were photographed with the imaging system at 4 and 24 h. Moreover, the Cy5 fluorescence was detected in the lung at different time points (0.5, 4, 8, 24, 48, and 72 h) after ALI mice injected with TAP nanoparticles by the IVIS Spectrum imaging system (PerkinElmer, Waltham, MA, USA). Additionally, lungs were fixed with 4% formaldehyde in a dark place. The tissues were labelled with collagen-I primary antibody and a FITC-labelled secondary antibody. Finally, DAPI was applied to label nucleus and lung tissues were imaged with a fluorescence microscope.

2.17. In vivo safety measurement

Healthy mice were intravenously injected with different nanoparticles for 24 h or 2 weeks and the blood was collected for detecting CRE, ALT and AST concentrations according to the kit instructions (Cat No. C011-2-1, C010-2-1, C009-2-1, Jiancheng, Nanjing, China). The livers were collected and stained with H&E for histopathological analysis.

2.18. Statistical analysis

All statistical analyses were performed using GraphPad Prism 8. One-way ANOVA followed by Dunnett's multiple comparisons test was used for comparison of more than two groups. Unpaired two-tailed Students' *t*-test was used for comparison of two groups, Data are presented as mean ± standard error of mean (SEM)

($n = 3$). A P value <0.05 is considered as significant difference ($^{*}P < 0.05$, $^{**}P < 0.01$, $^{***}P < 0.001$).

3. Results

3.1. The construction and characterization of TAP/pCas9-PAR2

The CRISPR-Cas9 plasmid alone fails to induce *PAR2* deficiency due to its large size, negative charge and instability *in vitro* or *in vivo*. For improving the efficiency of gene editing, the natural and anionic human serum albumin (HSA) with excellent biocompatibility was utilized to encapsulate CRISPR-Cas9 plasmid encoding *PAR2* sgRNA and Cas9 (*pCas9-PAR2*) in the assistance of PEI10K (Fig. 1A). In addition, the conjugation of collagen-binding peptide (CBP) endowed HSA nanoparticles with inflammatory site-targeting capacity (TAP/*pCas9-PAR2*), since abundant collages were exposed in the inflamed tissues[19]. Importantly, we discovered that pH was of most importance for HSA nanoparticle formula. HSA solution at pH 8 constructed nano-sized TAP/*pCas9-PAR2* particles at different N/P with average diameters of ~100 nm, whereas HSA solution at pH 4 or 6 formed large size particles (Fig. 1C and D, Supporting Information Table S3). It may because HSA solution at pH 8, which was much higher than the isoelectric point of HSA, led to the repulsion of anionic HSA molecules, consequently facilitating the formation of smaller nanoparticles[22,23]. As shown in Fig. 1B, PEI/*pCas9-PAR2* and AP/*pCas9-PAR2*, TAP/*pCas9-PAR2* nanoparticle exhibited strong Tyndall effects, suggesting its extraordinary colloidal property. The morphology of TAP/*pCas9-PAR2* also showed nearly spherical and uniform distribution by transmission electron microscopy (TEM) (Fig. 1E). Moreover, DLS analysis indicated that the average diameter of TAP/*pCas9-PAR2* was 105.59 ± 3.91 nm with a polydispersity index (PDI) of 0.209 ± 0.013, indicating relatively high uniformity, while the surface charge was negative with Zeta potential of −20 ± 0.78 mV (Fig. 1F). The SYBR Green staining tool was applied to detect unencapsulated plasmid after nanoparticle preparation, revealing that the drug loading capacity of TAP/*pCas9-PAR2* reached 0.195 ± 0.00003% and the encapsulation efficiency was 99.97 ± 0.014% (Fig. 1F). Additionally, the agarose gel electrophoresis result showed that TAP/*pCas9-PAR2* did not exhibit visual plasmid band compared to *pCas9-PAR2* alone, and there was nearly no plasmid band (unencapsulated *pCas9-PAR2*) detected after ultracentrifugation of TAP/*pCas9-PAR2* (Supporting Information Fig. S1), which was because plasmid concentration was too low to be detected. This result visually indicated the excellent encapsulation capacity of TAP/*pCas9-PAR2*.

More importantly, it has shown that TAP/*pCas9-PAR2* induced high transfection efficiency of GFP-*pCas9-PAR2* with or without DNase I, but *pCas9-PAR2* alone failed to induce such effects (Fig. 1G), suggesting the excellent protection of *pCas9-PAR2* by TAP/*pCas9-PAR2* under enzyme conditions. TAP/*pCas9-PAR2* has been also stable over 30 days since the particle size and polydispersity of nanoparticles were not significantly changed at room temperature for 30 days (Fig. 1H, I, and Supporting Information Table S4). These results suggest that TAP/*pCas9-PAR2* possessed outstanding physicochemical properties and preferably protected plasmid from nuclease degration, supporting its potency for gene drug delivery.

3.2. TAP/pCas9-PAR2 effectively delivered pCas9-PAR2 to evoke gene deficiency in vitro

Before gene editing by CRISPR-Cas9 in nucleus, the Cas9-*PAR2* plasmid should enter and effectively transfect cells. Near-infrared Cy5-labeled DNA was used instead of *pCas9-PAR2* to quantitatively evaluate the cell uptake of nanoparticles (Fig. 2B). The results showed TAP/*pCas9-PAR2* group markedly promoted uptake efficiency of *pCas9-PAR2* but *pCas9-PAR2* itself failed to enter cells. Importantly, TAP/*pCas9-PAR2* with *N/P* = 16:1 exhibited the most excellent efficiency of cell uptake among different *N/P* ratios. Nanoparticles with CBP (TAP/*pCas9-PAR2*) showed higher uptake efficiency than AP/*pCas9-PAR2* in RAW264.7 and A549 cells, suggesting that this collagen-binding peptide significantly assisted TAP/*pCas9-PAR2* to deliver plasmid into inflammatory cells.

To further investigate the transfection efficiency of TAP/*pCas9-PAR2*, we prepared *pCas9-PAR2* plasmid encoding green fluorescent protein (GFP) (GFP-*pCas9*-PAR2). The expression of GFP allowed the convenient readout of cell transfection efficiency. Under confocal fluorescence microscopy, *pCas9-PAR2* itself could not evoke any transfections by cells whereas GFP-tagged TAP/*pCas9-PAR2* exhibited strong green fluorescence, indicating that TAP/*pCas9-PAR2* intensively promoted cell transfections of *pCas9-PAR2* (Fig. 2A). Furthermore, consistent with cell uptake results, TAP/*pCas9-PAR2* at *N/P* = 16:1 triggered higher transfection efficiency than nanoparticles at other *N/P* ratios (8:1, 32:1), suggesting 16:1 was the optimized *N/P* ratio (Fig. 2C). Importantly, the CBP also dramatically enhanced cell transfections of nanoparticles, since TAP/*pCas9-PAR2* preferably improved ~30-fold transfection efficiency of *pCas9-PAR2* compared to plasmid alone and notably triggered ~1.5-fold higher transfection efficiency than AP/*pCas9-PAR2*. Although PEI polymer induced cell transfection of *pCas9-PAR2*, the transfection efficiency of TAP/*pCas9-PAR2* was remarkedly higher (~5-fold) than PEI/*pCas9-PAR2*, confirming TAP/*pCas9-PAR2* as a superior transfection reagent for CRISPR-Cas9.

The CRISPR-Cas9 plasmid encoding guide RNA targeting mouse *PAR2* (mF2RL1) and human *PAR2* (hF2RL1) were designed and constructed, respectively (Fig. 2D). T7E1 assay was applied to evaluate if the genome editing of CRISPR-Cas9 at targeted *PAR2* genome locus through recognizing and cleaving the mismatched DNA by T7EI endonuclease. Similar to lipofectamine 3000 group, two cleavage bands were clearly observed in the *PAR2* locus of TAP/*pCas9-PAR2* group with the cleavage efficiency of ~25.5% whereas *pCas9-PAR2* alone showed the original band without any cleavage bands (Fig. 2E). Additionally, Sanger sequencing results confirmed that indels were presented at *PAR2* loci with different mutation sites around protospacer adjacent motifs (PAMs) (Supporting Information Fig. S2), indicating the precise genome editing of TAP/*pCas9-PAR2*. Additionally, compared to naïve control, PEI/*pCas9-PAR2* and AP/*pCas9-PAR2*, RAW264.7 cells treated with TAP/*pCas9-PAR2* encoding mF2RL1 sgRNA triggered markable reductions in *F2rl1* (*Par2*) gene expression and PAR2 surface expression (Fig. 2F and G), while TAP/*pCas9-PAR2* encoding hF2RL1 gRNA also evoked strong *PAR2* gene editing in mRNA and surface expression levels in A549 cells (Supporting Information Fig. S3), suggesting successful gene editing of *PAR2*. Alternatively, cells were treated with TAP/*pCas9-PAR2* at different N/P ratios for 4 h and then replaced with fresh medium for further 44 h, which did not evoke

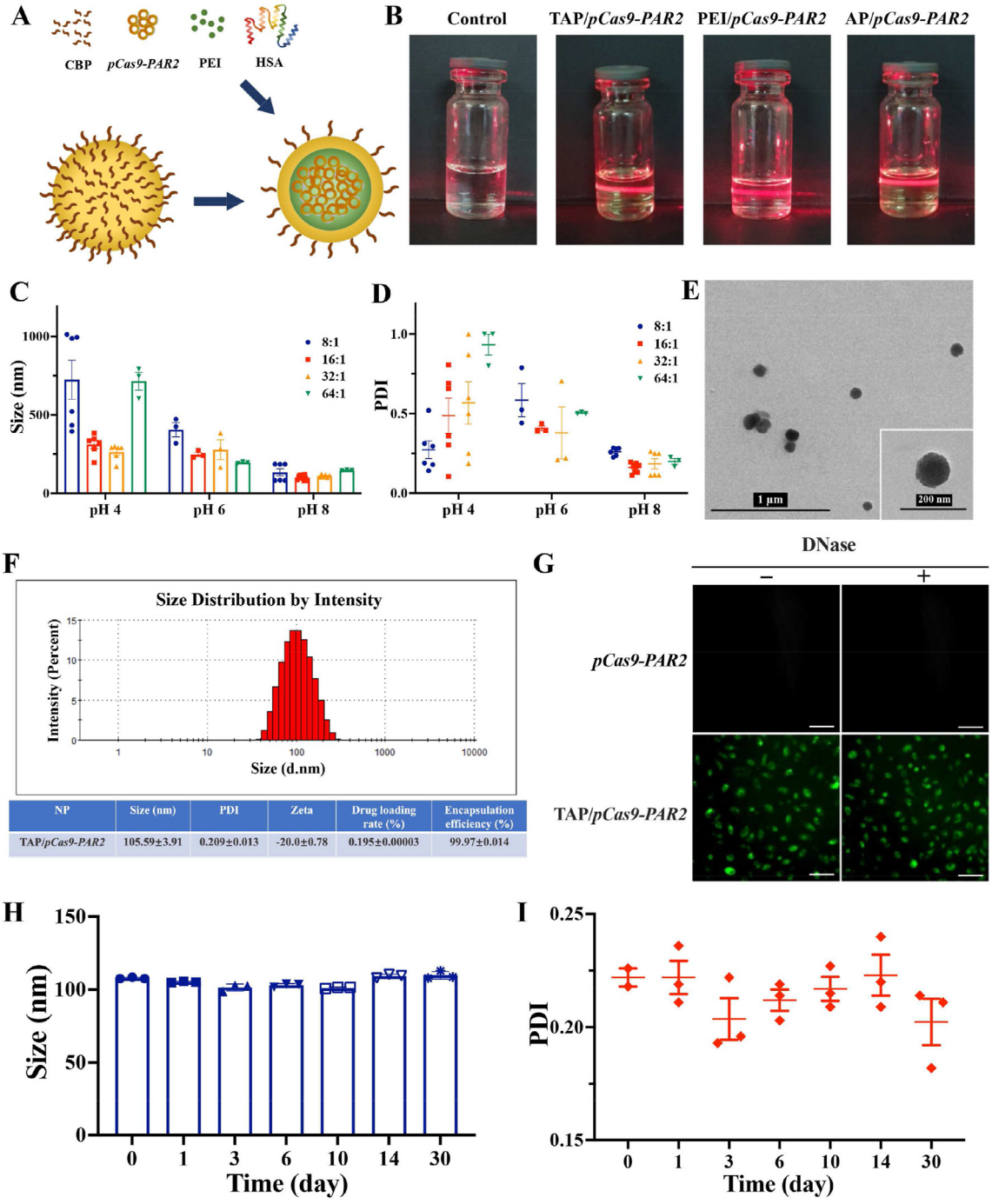

NP	Size (nm)	PDI	Zeta	Drug loading rate (%)	Encapsulation efficiency (%)
TAP/*pCas9-PAR2*	105.59±3.91	0.209±0.013	-20.0±0.78	0.195±0.00003	99.97±0.014

Figure 1 The physicochemical property of TAP/*pCas9-PAR2* nanoparticle. (A) The preparation of TAP/*pCas9-PAR2*; (B) The Tyndall effect of different nanoparticles; (C, D) The comparison of size and PDI of TAP/*pCas9-PAR2* under different N/P ratio and pH; (E) The TEM image of TAP/*pCas9-PAR2*. Scale bar = 1 μm (low-magnified); Scale bar = 200 nm (high-magnified); (F) The Size, polydispersity index (PDI), Zeta, drug loading rate and encapsulation efficiency of TAP/*pCas9-PAR2*; (G) TAP/*pCas9-PAR2* protected cell transfection of *pCas9-PAR2* from DNase I degration in RAW264.7. Scale bar = 50 μm; (H, I) The stability of TAP/*pCas9-PAR2* during one month by detecting changes in the size (H) and PDI (I) of nanoparticles.

obvious cell toxicity, while TAP/*pCas9-PAR2* also elicited excellent cell viability after 48 h incubation, supporting the superior safety of TAP nanoparticles (Fig. 2H, Supporting Information Fig. S4). Taken together, TAP/*pCas9-PAR2* at *N/P* ratio = 16:1 could efficiently deliver CRISPR-Cas9 plasmid into cells and successfully evoke *PAR2* gene editing *in vitro*.

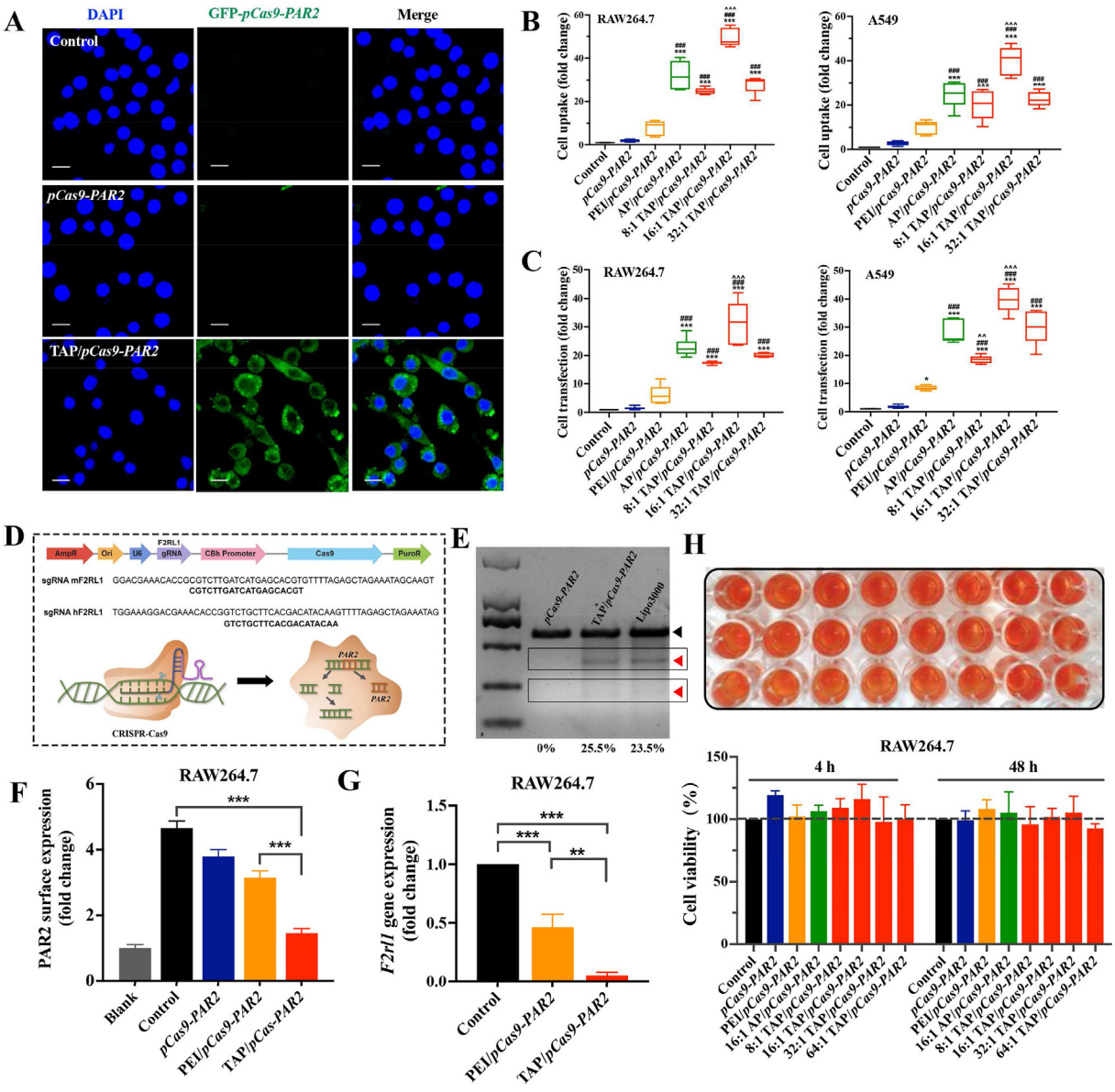

Figure 2 The cell uptake, transfection and gene editing of TAP/*pCas9-PAR2*. (A) Representative confocal images of cell transfection of *pCas9-PAR2* and TAP/*pCas9-PAR2*. DAPI: blue, nucleus. GFP: green, GFP-*pCas9-PAR2*. Scale bar = 10 μm; (B) Cell uptake efficiency of nanoparticles with different N/P ratios in RAW264.7 and A549 cells; (C) Transfection efficiency of NPs with different N/P ratios in RAW264.7 and A549 cells; (D) The CRISPR/Cas9 plasmid encoding different guide RNA sequences for targeting mouse *PAR2* (mF2RL1) or human *PAR2* (hF2RL1); (E) Gene editing of *PAR2* locus after cells treated with *pCas9-PAR2*, TAP/*pCas9-PAR2* or lipofectamine 3000 were detected by T7EI assay. The original PCR product size is 555 bp; (F) For estimating gene editing by CRISPR/Cas9, RT-PCR technique was applied for detecting *F2rl1* (*Par2*) gene expression in RAW264.7 cells; (G) The cell surface expression of PAR2 was detected among different groups by FACS. (H) The cell viability of cells treated with different nanoparticles were detected for evaluating their toxicity. Cells were treated with nanoparticles at different N/P ratios for 4 h and replaced with complete medium for further 44 h or were directly incubated with nanoparticles for 48 h. There was no statistical significance among all groups. $^{*}P < 0.05$, $^{**}P < 0.01$, $^{***}P < 0.001$ *vs.* LPS+2f. $^{\#\#\#}P < 0.001$ *vs. pCas9-PAR2*. $\hat{}P < 0.01, \hat{}P < 0.001$ *vs.* AP/*pCas9-PAR2*.

3.3. PAR2 deficiency by TAP/pCas9-PAR2 mitigated PAR2-induced paw edema and non-specific paw edema in vivo

Apart from *in vitro PAR2* knockout by TAP/CRISPR-Cas9, we further evaluated its capacity of gene editing *in vivo*. The pharmacokinetics of TAP/*pCas9-PAR2* was firstly investigated by detection of the average plasma concentration of Cy5-DNA after intravenous injection of nanoparticles into healthy mice (Fig. 3A). These pharmacokinetic parameters were also summarized in Supporting Information using two-compartment model analysis. Results showed that the distribution half-life ($t_{1/2\alpha}$) of TAP/*pCas9-PAR2* was 3.5-fold higher than *pCas9-PAR2*, while TAP/*pCas9-PAR2* robustly prolonged the elimination half-life ($t_{1/2\beta}$) of *pCas9-PAR2 in vivo* by ~30 h. Furthermore, AUC_{0-t} of TAP/*pCas9-PAR2* treatment exhibited ~3-fold higher than *pCas9-PAR2*, and TAP/*pCas9-PAR2* with enhanced peak plasma

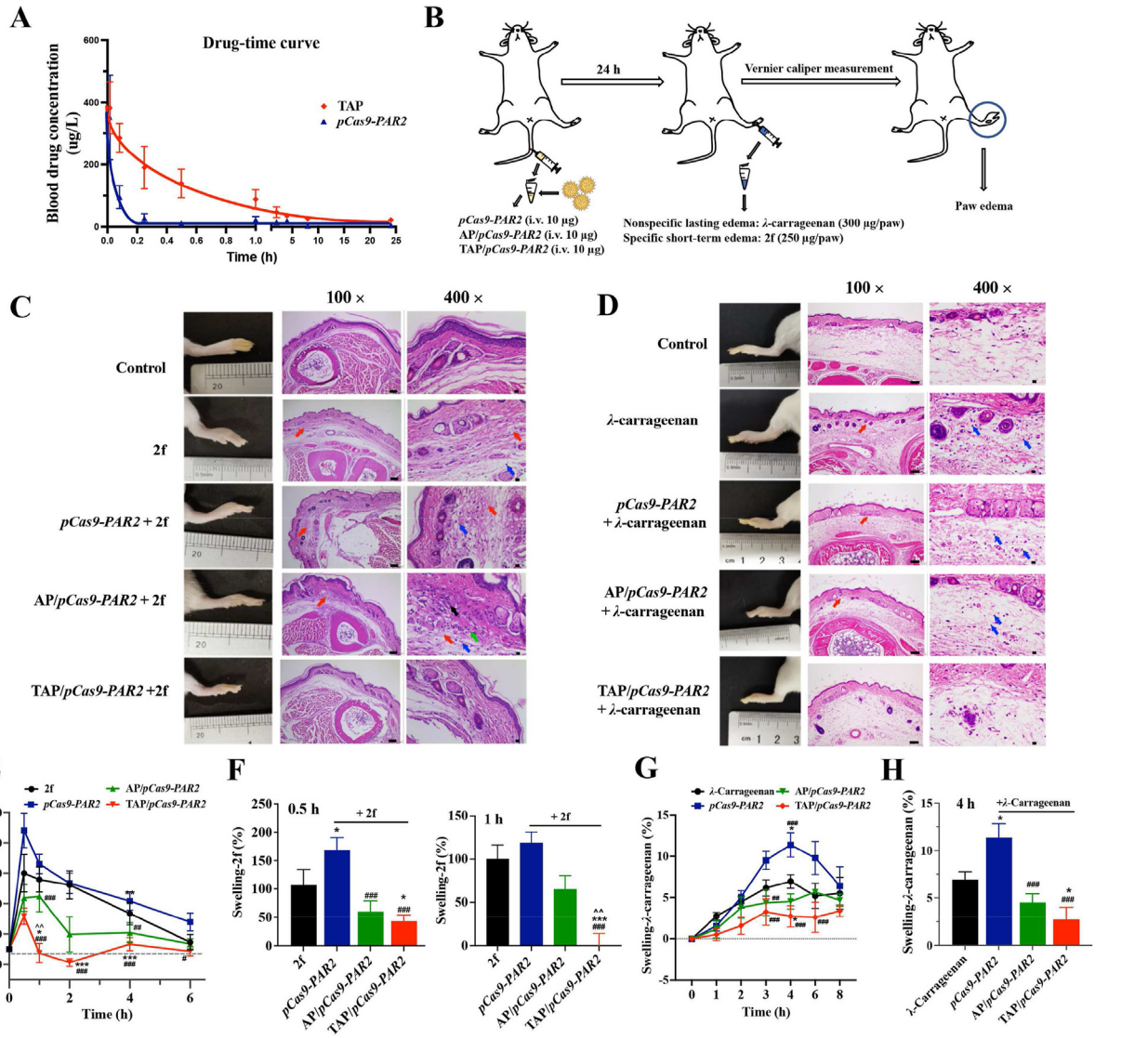

Figure 3 TAP/*pCas9-PAR2* initiated *in vivo* gene editing to alleviate PAR2-specific and non-specific paw edema. (A) Pharmacokinetic study of TAP/*pCas9-PAR2* in healthy mice; (B) Schematic diagram of paw edema experiments; (C, D) The paw edema images and further H&E staining analysis of nanoparticle treatment groups in 2f-LIGRL-NH_2-induced specific short-term paw edema at 0.5 h (C) and λ-carrageenan-stimulated paw edema model at 4 h (D). Red arrow: edema, blue arrow: lymphocytes, green arrow: dead collagen fibers, black arrow: neutrophils. Scale bar = 100 μm (100 ×), scale bar = 10 μm (400 ×); (E) Time courses of nanoparticles-treated PAR2-specific short-term paw edema; (F) The comparison of different treatments for PAR2-specific paw edema models at 0.5 and 1 h; (G) Time courses of nanoparticles-treated non-specific paw edema; (H) The comparison of different treatments in non-specific paw edema models at 4 h, $^{*}P < 0.05$, $^{**}P < 0.01$, $^{***}P < 0.001$ *vs.* 2f or λ-carrageenan, $^{\#}P < 0.05$, $^{\#\#}P < 0.01$, $^{\#\#\#}P < 0.001$ *vs. pCas9-PAR2*, $^{\wedge}P < 0.01$ *vs.* AP/*pCas9-PAR2*.

concentration and persistent time showed ~100-fold increase of $AUC_{0-\infty}$ for *pCas9-PAR2*. Therefore, TAP/*pCas9-PAR2* possessed superior pharmacokinetic properties and significantly improved the bioavailability of *pCas9-PAR2* for effective gene editing.

Alternatively, we constructed two mice paw edema models as traditional animal inflammatory models which were highly related to PAR2[24,25]. The classic PAR2 agonist, 2-furoyl-LIGRL-NH_2 (2f-LIGRL-NH_2, 2f), stimulated PAR2-specific paw edema as a short-term model, while λ-carrageenan that is a soluble complex extracted from carrageenaceae can evoke non-specific paw edema modeling (Fig. 3B). The swelling degree were monitored and measured using electronic vernier calipers at fixed intervals over 8 h, discovering that it peaked at 0.5 h for PAR2-specific paw edema and at 4 h for non-specific paw edema, and rapidly decreased after peak time (Fig. 3E and G). To precisely investigate the anti-inflammatory effects, nanoparticles were administrated intravenously 24 h before stimulation of paw edema, which could guarantee enough time for *PAR2* gene editing. Results showed that TAP/*pCas9-PAR2*-treated mice remarkedly alleviated PAR2-specific and non-specific foot swelling, which were more potent than AP/*pCas9-PAR2* group (Fig. 3C−H). It is worth mentioning that *pCas9-PAR2* exhibited a stronger paw edema response than stimulators probably due to plasmid-induced inflammation, suggesting that TAP nanoparticle could prevent immunogenicity of *pCas9-PAR2*. Meanwhile, H&E staining results showed that no

obvious edema or inflammatory infiltration was observed in TAP/*pCas9-PAR2* and control groups (Fig. 4C and D), but *pCas9-PAR2* alone had the most severe inflammatory infiltration, which also reflected the advantage of using human serum albumin as nanoparticles with low toxicity. These results indicated that TAP/*pCas9-PAR2* possessed the extraordinary capacity of *in vivo PAR2* gene editing and potential therapeutical effects for PAR2-mediated inflammatory diseases.

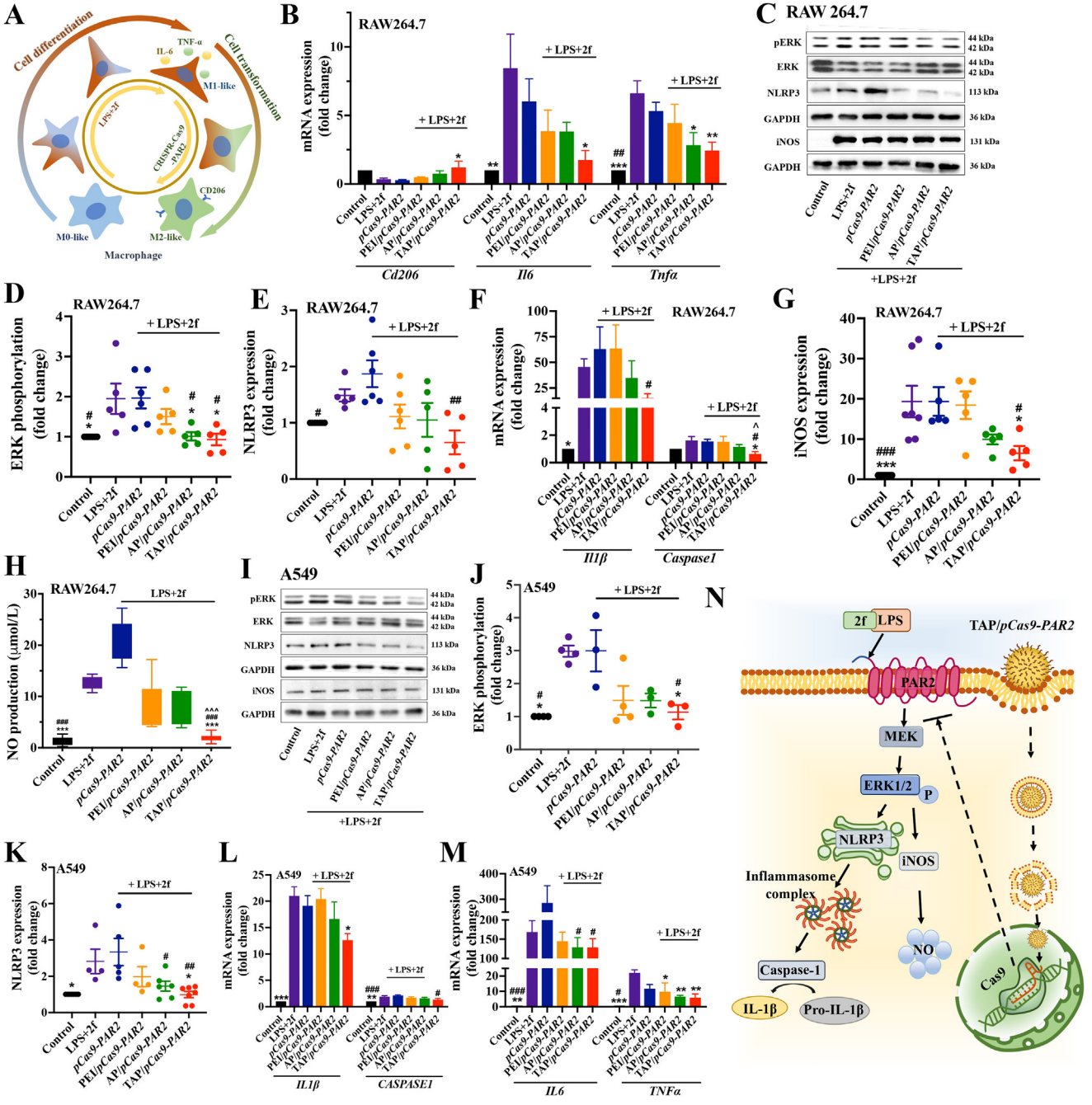

Figure 4 TAP/*pCas9-PAR2* modulated macrophage polarization, proinflammatory cytokine expressions through ERK/NLRP3/Caspase-1/IL-1β and NO/iNOS signalling. (A) A schematic diagram for PAR2-mediated macrophage polarization; (B) The changes in mRNA levels of *Cd206*, *Il6*, and *Tnfα* after RAW264.7 cells were treated with different nanoparticles detected by RT-PCR; (C−E) The changes in protein expressions of ERK, phosphorylated ERK and NLRP3 after RAW264.7 cells were treated with different nanoparticles detected by Western blotting; (F) The comparison of mRNA levels of *Il1β* and *Caspase1* after RAW264.7 cells were treated with different treatments; (G) The protein expression of iNOS in RAW264.7 cells after different treatments; (H) The changes in NO productions after RAW264.7 cells with different treatments; (I−K) The changes in protein expressions of ERK, phosphorylated ERK and NLRP3 after A549 cells were treated with different nanoparticles. (L, M) The changes in mRNA levels of *IL6*, *TNFα*, *IL1β* and *CASPASE1* after A549 cells were treated with different nanoparticles; (N). The schematic diagram of TAP/*pCas9-PAR2*-mediated downstream inflammatory signalling pathways. $^{*}P < 0.05$, $^{**}P < 0.01$, $^{***}P < 0.001$ *vs.* LPS+2f. $^{\#}P < 0.05$, $^{\#\#}P < 0.01$, $^{\#\#\#}P < 0.001$ *vs. pCas9-PAR2*. $\hat{}P < 0.05$, $\hat{}P < 0.001$ *vs.* AP/*pCas9-PAR2*.

3.4. *PAR2 gene editing by TAP/pCas9-PAR2 evoked anti-inflammatory activity via alleviating ERK/NLRP3/caspase-1/IL-1β and NO/iNOS signalling*

In attempt to probing underlying mechanism of TAP/*pCas9-PAR2*-mediated anti-inflammatory capacity, we further investigated intracellular signalling pathways and responses. It has been widely reported that macrophages exhibited different types, including M0 macrophages, M1 pro-inflammatory macrophages and M2 anti-inflammatory macrophages[26]. During inflammatory progress, different macrophages initiate transformation and polarization that could be a crucial indicator for inflammation. Importantly, TNF-α and IL-6 cytokine are M1 macrophages-related cytokines whereas CD206 represents M2-like macrophages (Fig. 4A). As shown in Fig. 4A and B, LPS and 2f-LIGRL-NH_2 (2f) significantly attenuated mRNA expressions of *Cd206* and enhanced *Tnfα* and *Il6* expressions, suggesting that LPS plus PAR2 activation promoted M2 to M1 macrophage polarization. Moreover, *TAP/pCas9-PAR2*, but not *pCas9-PAR2*, PEI/*pCas9-PAR2* or AP/*pCas9-PAR2*, evoked *PAR2* gene editing to robustly mitigate PAR2-induced enhancement of *Tnfα* and *Il6* expressions (∼3.5-fold) as well as reduction of *Cd206* expressions (∼2.5-fold) in RAW264.7 cells. It indicated that PAR2 promoted transformation of M2 to M1 proinflammatory macrophages and *PAR2* deficiency induced by TAP/*pCas9-PAR2* remarkably reversed macrophage polarization, exerting superior anti-inflammatory responses.

Additionally, we discovered that PAR2-mediated inflammation was highly related to ERK and NLRP3 inflammasome signalling. Although ERK signalling was one of the most common pathways modulated by PAR2 activation, the relationship between PAR2 and NLRP3 has been rarely reported. LPS and 2f-LIGRL-NH_2 significantly initiated ERK phosphorylation and NLRP3 expression (∼2-fold increase) in both RAW264.7 (Fig. 4C−E) and A549 cells (Fig. 4I−K). Importantly, PAR2-evoked ERK phosphorylation was time-dependent, which peaked at 30 min in RAW264.7 cells and at 10 min in A549 cells (Supporting Information Fig. S5). TAP/*pCas9-PAR2* could not only dramatically deliver CRISPR-Cas9 to edit *PAR2* gene for alleviating PAR2-induced phosphorylated ERK and NLRP3 expressions, but also triggered much more potent inhibitions than PEI/*pCas9-PAR2* and AP/*pCas9-PAR2*. Moreover, Caspase-1 and IL-1β as NLRP3 inflammasome downstream proteins were detected for supporting NLRP3 signalling pathway[27,28]. Unsurprisingly, as shown in Fig. 4F and L, TAP/*pCas9-PAR2* attenuated PAR2-induced mRNA expression levels of *Caspase1* and *Il1β* compared to simulators and *pCas9-PAR2* group in RAW264.7 and A549 cells, confirming the active participation of NLRP3/Caspase-1/IL-1β signalling. TAP/*pCas9-PAR2*, but not *pCas9-PAR2*, PEI/Cas9-*PAR2* and AP/Cas9-*PAR2*, also markedly prevented PAR2-mediated proinflammatory cytokine expressions, *TNFα* and *IL6*, in A549 cells, further indicating its strong anti-inflammatory activity (Fig. 3M). Furthermore, PAR2 activation dramatically facilitated ∼20-fold enhancement of iNOS protein expressions in RAW264.7 (Fig. 4G) and ∼2-fold increase in A549 cells (Supporting Information Fig. S6), while LPS and 2f-LIGRL-NH_2 promoted ∼14-fold increase in nitric oxide (NO) production (Fig. 4H). Compared to *pCas9-PAR2*, PEI/*pCas9-PAR2* and AP/*pCas9-PAR2*, TAP/*pCas9-PAR2* markedly mitigated PAR2-induced NO/iNOS pathways, confirming that TAP/*pCas9-PAR2* with CBP could inhibit PAR2-mediated NO/iNOS signalling. Importantly, consistent with previous results, *pCas9-PAR2* stimulated inflammation-related cytokine release, protein expression and NO productions, suggesting plasmid itself might stimulate inflammatory responses. TAP nanoparticles could prevent *pCas9-PAR2* from such spontaneous inflammation and trigger anti-inflammatory activity.

Taken together, TAP/*pCas9-PAR2* could enter and transfect cells to initiate *PAR2* gene editing by CRISPR-Cas9, and then alleviated PAR2 and LPS-induced ERK/NLRP3/Caspase-1/IL-1β signalling and NO/iNOS pathways, consequently mitigating PAR2-induced inflammatory responses (Fig. 4N).

3.5. *PAR2 deficiency by TAP/pCas9-PAR2 alleviated PAR2-mediated acute lung inflammation in vivo*

We also probed the novel value of PAR2 and anti-inflammatory effects of TAP/*pCas9-PAR2* in another mice inflammatory model. Acute lung inflammation (ALI) is one of the most common LPS-induced inflammation related to cytokine storm and lung inflammation. Our study firstly investigated the relationship between PAR2 and ALI through LPS plus 2f-LIGRL-NH_2-induced lung inflammation (Fig. 5A). The addition of 2f-LIGRL-NH_2 into LPS could robustly enhance LPS-induced lung inflammation, uncovering that PAR2 activation worsened ALI progression (Fig. 5). More importantly, ALI could be initially induced at 2 h while the severity of this disease probably peaked at 24 or 48 h, and then decreased. Meanwhile, CRISPR-Cas9 plasmid required at least 24 h for transfection and gene editing of *PAR2*. Therefore, we used LPS+2f to stimulate initial ALI at 2 h and then added nanoparticles for investigating *PAR2* gene editing in treating ALI progression. Before evaluating therapeutic efficacy, the *in vivo* biodistribution of nanoparticles was investigated for verifying inflamed lung-targeting efficiency of TAP/*pCas9-PAR2* (Supporting Information Fig. S7A−S7C). At 4 h after intravenous injection of Cy5-labeled nanoparticles, it was observed that TAP/*pCas9-PAR2* groups with addition of CBP that was the collagen-targeting peptide possessed higher fluorescence intensity in the lung tissue than AP/*pCas9-PAR2*, whereas there was no fluorescence in lung section from mice treated with *pCas9-PAR2*. Interestingly, TAP/*pCas9-PAR2* group still maintained a high fluorescence intensity in lung tissue, but the fluorescence signal of AP/*pCas9-PAR2* was gradually decreased after 24 h. These results could be explained by the high affinity of collagen-binding peptide CBP for abundant collagens at inflammation sites. When acute lung inflammation occurs in mice, the intercellular substance secretes collagen to repair, and consequently excessive collagen aggregation promotes pulmonary fibrosis[19]. As expected, TAP/*pCas9-PAR2* group exhibited strong Cy5 fluorescence intensity (red) which was preferably co-located with the green fluorescence of collagens in inflamed lungs whereas *pCas9-PAR2* failed to trigger such effects (Fig. 5B), further supporting the superior targeting efficiency of TAP/*pCas9-PAR2*. Moreover, AP/*pCas9-PAR2* without CBP largely induced the half-reduction of mean fluorescence intensity or fluorescence area percentages compared to TAP/*pCas9-PAR2* (Fig. 5B, Fig. S8), confirming that CBP assisted abundant TAP nanoparticles to deeply arrive at the damaged pulmonary sites *via* binding to pathological collagens. It also supported that TAP nanoparticles could trigger the abundant accumulations of *pCas9-PAR2* and Cas9 positive cells for efficient gene editing *in vivo*. More importantly, we detected Cy5 fluorescence in the lung at different time points (0.5, 4, 8, 24, 48, and 72 h) after ALI mice injected with TAP nanoparticles for revealing the dynamic manner of plasmid delivery in lungs (Fig. 5C,

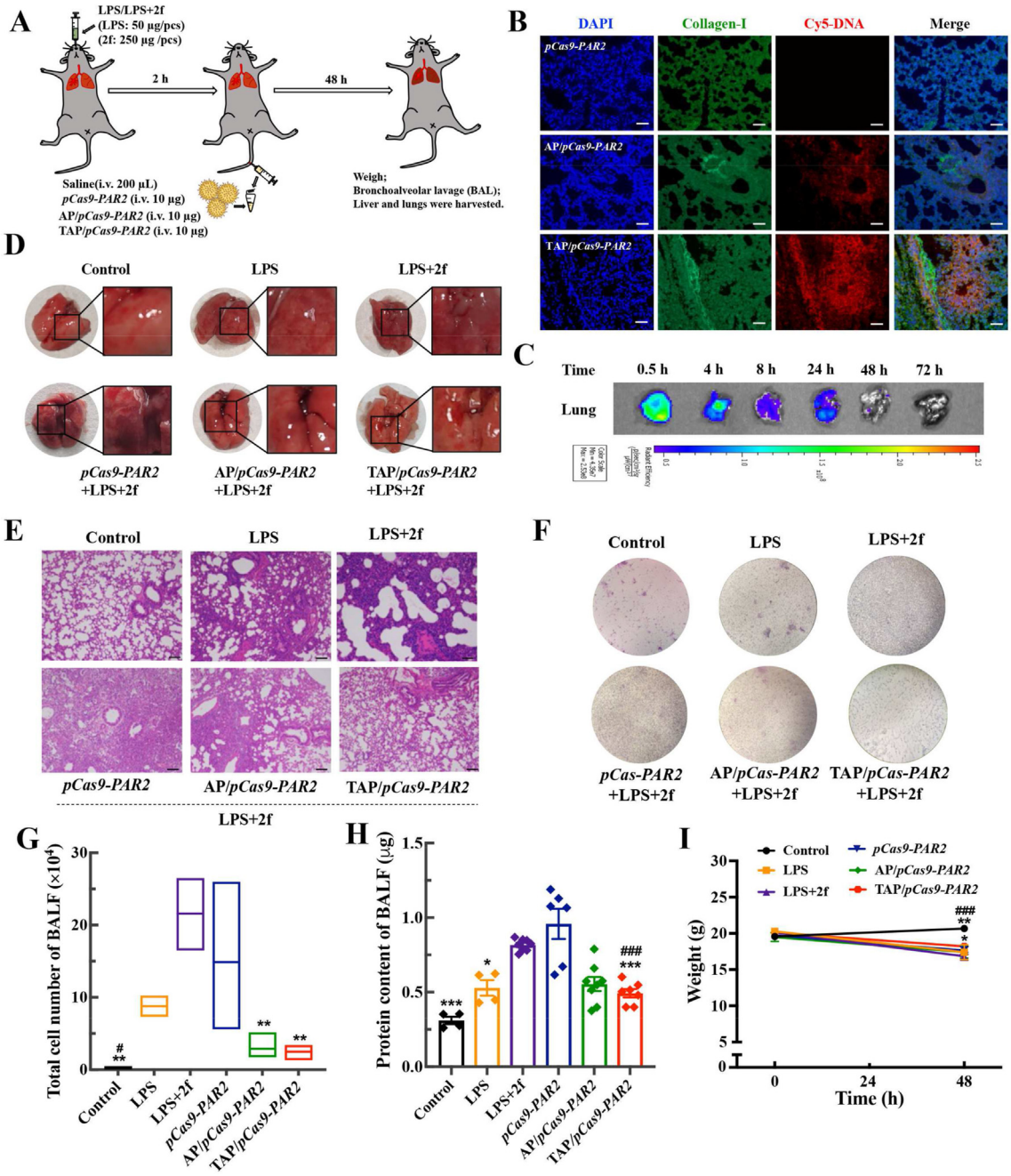

Figure 5 TAP/*pCas9-PAR2* evoked *PAR2* deficiency to mitigate acute lung inflammation. (A) A schematical diagram of LPS+2f-induced acute lung inflammation model and nanoparticles administration; (B) The detection of Cy5-labelled nanoparticles co-located with collagen (green) in inflamed lungs of ALI mice injected with different treatments by an immunofluorescence assay. Cy5-DNA as a fluorescent substitution for *pCas9-PAR2*. Scale bar = 50 μm; (C) The Cy5 fluorescence was detected in the lung at different time points (0.5, 4, 8, 24, 48, and 72 h) after ALI mice injected with TAP nanoparticles; (D) The comparison of lung tissue images of LPS+2f-induced ALI mice treated with different nanoparticles; (E) The H&E staining of inflamed lung tissues. The scale bar = 100 μm (100 ×); (F, G) Gisam staining of cells and cell number count in the BALF; (H) Total protein content in the BALF; (I) The changes in body weight of ALI mice with different treatment groups. There was no statistical significance between AP/*pCas9-PAR2* and TAP/*pCas9-PAR2* group. $^{*}P < 0.05$, $^{**}P < 0.01$, $^{***}P < 0.001$ *vs.* LPS+2f. $^{\#}P < 0.05$, $^{\#\#}P < 0.01$, $^{\#\#\#}P < 0.001$ *vs. pCas9-PAR2*.

Fig. S7D). Results uncovered that TAP nanoparticles could deliver *pCas9-PAR2* to the lung at 0.5 h, while the fluorescence was largely decreased at 48 h and totally could not be detected at 72 h. It suggested that TAP/*pCas9-PAR2* could rapidly arrive at the inflamed lung for initiating gene editing of CRISPR-Cas9, and its persistent time of 24～48 h could guarantee sufficient *PAR2* deficiency since it was enough for plasmid transfection. Therefore, TAP/*pCas9-PAR2* with CBP targeting the increased collagen in

lungs exhibited higher retention and targeting capacity in the inflamed lung, which is conducive to the accurate *PAR2* gene editing and low side effects *in vivo*.

More importantly, it was observed that the LPS, LPS+2f and *pCas9-PAR2* treatment group elicited pulmonary edema, and surfaces of lung tissues were congested and covered with blood clots (Fig. 5D). However, the lung of mice treated with TAP/*pCas9-PAR2* was normal and smooth without congestion. Furthermore, the H&E analysis validated that lung tissues of LPS, LPS+2f, *pCas9-PAR2* and AP/*pCas9-PAR2* group were dense due to alveolar injury and inflammatory cell infiltration, whereas TAP/*pCas9-PAR2* exhibited loose and regular lung tissues (Fig. 5E). More importantly, the *in vivo* anti-inflammatory effects of TAP/*pCas9-PAR2* on LPS+2f-induced ALI was compared with a commercial carrier, Lipofectamine 3000, as a positive control (Supporting Information Fig. S9). Results showed that TAP/*pCas9-PAR2* exhibited smoother lungs without any edema or congestion than the lipofectamine 3000 group while H&E results uncovered more normal and looser lung tissues in TAP/*pCas9-PAR2* group, although both groups triggered potent anti-inflammatory responses. When the lungs of mice are injured, immune cells (macrophages, neutrophils, and lymphocytes) are mobilized to accumulate in the lungs to engulf bacteria and suppress inflammatory response, but they also induce an inflammatory infiltration. As shown in Fig. 5F−G, LPS and 2f-LIGRL-NH_2 robustly increased cell number in BALF, while AP/*pCas9-PAR2* and TAP/*pCas9-PAR2* treatment largely abolished their effects compared to LPS+2f group. Moreover, due to a large amount of protein accumulation in inflamed lungs, the protein secretion content in mouse bronchoalveolar lavage fluid (BALF) can characterize the pathological status of ALI mice. As shown in Fig. 5H, the protein content of mice treated with LPS+2f was increased by 54% compared to LPS-induced ALI, indicating that PAR2 activation could enhance protein secretion conducive to acute lung inflammation. AP/*pCas9-PAR2* and TAP/*pCas9-PAR2* group were remarkably decreased by 32% and 40% in protein production in BALF compared to LPS+2f group. Alternatively, although mice with nanoparticle treatments showed slight weight loss, TAP/*pCas9-PAR2* only exhibited the least weight loss (∼5%) among all groups and there was ∼20% weight loss in LPS+2f group ($^*P < 0.05$), suggesting that TAP/*pCas9-PAR2* significantly improved body weight of ALI mice (Fig. 5I). We also detected the lung wet/dry weight ratio which was evaluated to indicate the pulmonary edema. However, 2f + LPS increased wet/dry weight ratio from ∼4.2 to 4.5 without statistical significance, and TAP/*pCas9-PAR2* treatment had no obvious effect (Supporting Information Fig. S10). It was probably because the experiment time of our ALI model (48 h) was longer than ALI model at 24 h, initiating the partial transformation of pulmonary edema into injury which led to less observation in the lung edema. There was no significant difference of lung edema (wet/dry ratio) among all groups. Therefore, it firstly revealed that PAR2 activation contributed to ALI and TAP/*pCas9-PAR2* possessed *PAR2* deficiency to trigger anti-inflammatory effects in lung inflammatory diseases.

3.6. TAP/pCas9-PAR2 attenuated acute lung inflammation via NLRP3 inflammasome/IL-1β and iNOS signalling

For ALI, the massive cytokine releases are directly related to pneumonia and may worsen into the cytokine storm. The proinflammatory cytokine productions in BALF were detected to further investigate inflammatory status (Fig. 6A−C). Compared with control, LPS and 2f-LIGRL-NH_2 group robustly enhanced TNF-α, IL-6, and IL-1β secretion by 20-, 8- and 5-fold, respectively, which were also more potent than LPS alone, indicating PAR2-mediated serious inflammatory infiltration in lungs. Meanwhile, TNF-α, IL-6 and IL-1β cytokine releases in TAP/*pCas9-PAR2* group were significantly down-regulated by 66%, 85% and 65%, respectively, compared to LPS+2f group, preventing the deterioration of inflammatory response. Alternatively, key protein expressions in lung tissues were evaluated to verify molecular mechanism of the inhibitory effect of TAP/*pCas9-PAR2* in inflammation *in vivo*. Importantly, lung tissues from TAP/*pCas9-PAR2* group exhibited two cleavage bands with the cleavage efficiency of ∼22.0%, which was similar to lipofectamine 3000 group, suggesting the efficient *in vivo* gene editing of *PAR2* (Supporting Information Fig. S11). As shown in Fig. 6D, E, and G, LPS and LPS+2f group significantly enhanced the protein levels of NLRP3 and iNOS, whereas TAP/*pCas9-PAR2* markedly decreased *PAR2* expression *via* CRISPR-Cas9 editing and subsequently alleviated NLRP3 and iNOS signalling. These results further supported PAR2-mediated inflammatory responses *via* NLRP3 inflammasome and iNOS signalling *in vivo*.

Finally, we investigated *in vivo* safety and biocompatibility of TAP/*pCas9-PAR2* nanoparticles in healthy mice. According to the *in vivo* biodistribution results of nanoparticles (Supporting Information Fig. S7A−S7C), apart from inflamed lung tissues, some TAP/*pCas9-PAR2* were accumulated in liver and kidney tissues. We detected the possible toxicity of nanoparticles in liver and kidney. As shown in Fig. 6F, the H&E staining showed that there was no significant toxic damage in liver tissues after nanoparticles were intravenously injected into mice for 24 h. More importantly, the systematic toxicity of nanoparticles was also evaluated after two-week administration. As shown in Supporting Information Fig. S12, there was no obvious toxicity in heart, liver, spleen, lung and kidney tissues of TAP/*pCas9-PAR2* group. TAP/*pCas9-PAR2* did not exhibit significant differences from control and *pCas9-PAR2* group in AST and ALT as serum liver function indicators and CRE as a renal function index (Fig. 6H−J), further suggesting TAP/*pCas9-PAR2* did not induce severe two-week toxicity. These results indicated that this HSA-based nanoparticle exhibited low *in vivo* short-term toxicity, suggesting its potential therapeutical application in treatment of inflammatory diseases.

4. Discussion

Due to the outbreak of COVID-19 pandemic, exploring forceful therapeutical strategies for pulmonary inflammation becomes increasingly emergent and concerned[6]. GPCRs account for ∼40% of molecular targets for approved clinical drugs, since they including PAR2 are widely distributed through human body and vigorously involve in a variety of physiological responses and diseases[29]. Although the principal role of PAR2 in diseases is the robust modulation of inflammatory responses[9], PAR2 has rarely been probed in lung inflammatory progression. Interestingly, it has been reported that proteases, such as TMPRSS2, cathepsin, elastase, and protease-induced tissue damages are highly associated with the pathogenesis of lung inflammatory diseases[4,30], while PAR2 is a membrane receptor primarily activated by proteases to evoke signal transductions[8], suggesting possible relationship of PAR2 and pulmonary diseases. This work focused on revealing the novel role of PAR2 and underlying molecular mechanism in lung inflammatory diseases.

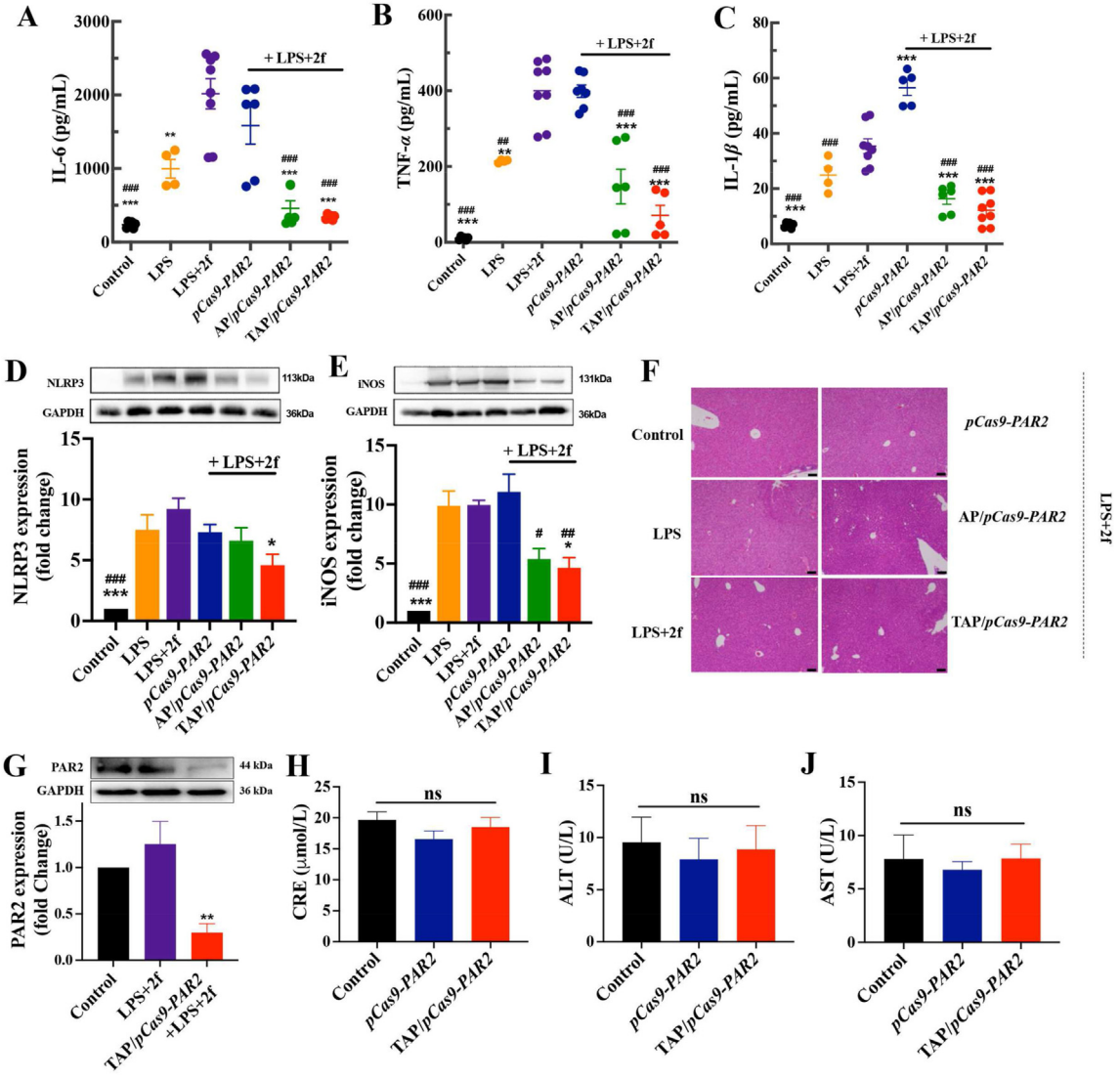

Figure 6 TAP/*pCas9-PAR2* mitigated cytokine releases and lung inflammation *via* NLRP3 inflammasome and iNOS signalling with low short-time systemic toxicity. (A−C) IL-6, TNF-α and IL-1β productions in the BALF from ALI mice with different nanoparticle administrations were examined by ELISA; (D, E) The protein expressions of NLRP3 and iNOS in lung tissues from ALI mice with different administrations; (F) The H&E staining of liver tissues from ALI mice with different administrations. The scale bar = 100 μm (100 ×); (G) PAR2 expressions in lung tissues from ALI mice with different administrations after 24 h; (H−J) The level of CRE, AST and ALT in serum from ALI mice with different administrations after 2 weeks. $^{*}P < 0.05$, $^{**}P < 0.01$, $^{***}P < 0.001$ *vs.* LPS+2f. $^{\#}P < 0.05$, $^{\#\#}P < 0.01$, $^{\#\#\#}P < 0.001$ *vs. pCas9-PAR2*. ns: no significant difference.

Unlike traditional PAR2 inhibitors in previous studies, we firstly constructed an all-in-one CRISPR-Cas9-*PAR2* sgRNA plasmid (*pCas9-PAR2*) for investigating PAR2 blockade in diseases. CRISPR-Cas9 as a powerful and superior genome-editing technique can precisely evoke gene editing[11], while gene therapy exhibits abundant advantages over chemotherapeutic agents, such as extraordinary specificity and targeting[31,32], suggesting that *PAR2* deficiency by CRISPR-Cas9 could be a novel candidate for PAR2-based therapeutics. However, a key restriction for gene therapy is the lack of a delivery system for drug safety and efficacy. While cationic nanoparticles have been widely applied for delivering CRISPR-Cas9 system, high toxicity still limited their applications[14,33,34]. Apart from cationic nanoparticles, it has been proposed that the cell membrane is relatively dynamic and negatively-charged nanoparticles can be adhere to the positive-charged position of cells[35], indicating anionic nanoparticles also elevate cell uptake and transfection efficacy of gene drugs. Our study firstly utilized HSA-based nanoparticles to condense and encapsulate *pCas9-PAR2* (TAP/*pCas9-PAR2*) with excellent particle size and stability, whereas *pCas9-PAR2* itself exhibited large size and was readily degraded by DNase (Fig. 1). Moreover, TAP/*pCas9-PAR2* successfully facilitated *pCas9-PAR2* to enter and transfect inflammatory cells, consequently provoking *PAR2* knockout by CRISPR-Cas9 *in vitro* and *in vivo* (Figs. 2 and 6G, Fig. S11). Alternatively, mouse paw edema model as standard PAR2-mediated inflammatory model was used for verifying *PAR2* deficiency by TAP/*pCas9-PAR2* *in vivo*. TAP/*pCas9-PAR2*, but not *pCas9-PAR2*, robustly eliminated 2f-LIGRL-NH_2- or λ-carrageenan-induced paw edema, confirming that TAP/*pCas9-PAR2* precisely evoked gene editing of *PAR2* to prevent inflammatory responses *in vivo*. Therefore, we successfully

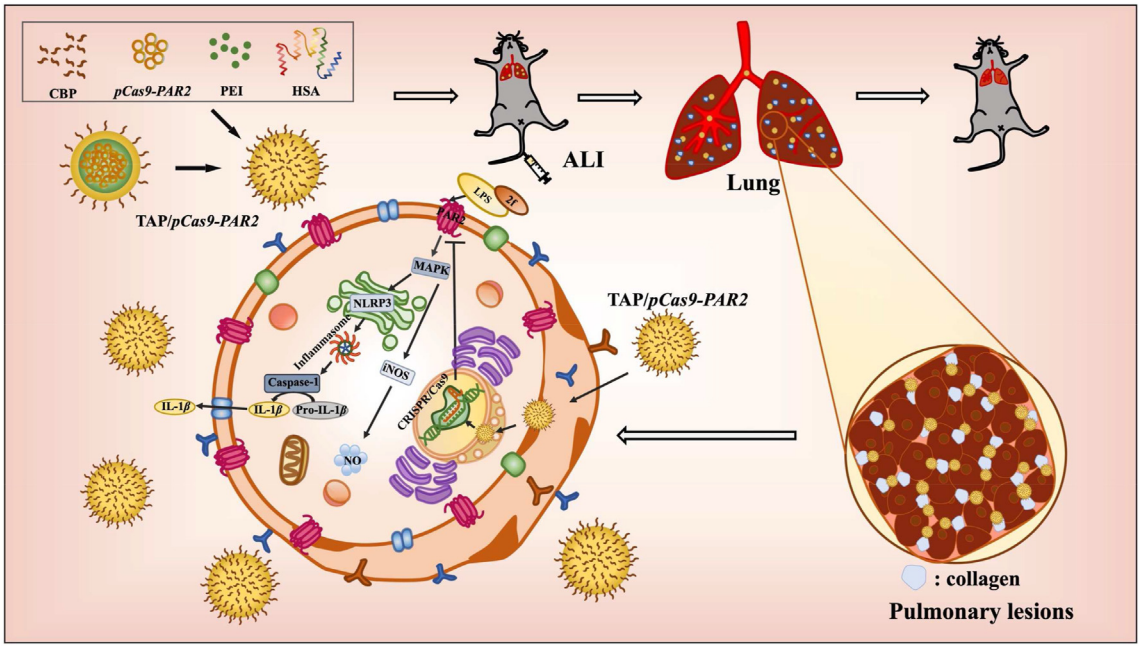

Figure 7 Schematical diagram of TAP/*pCas9-PAR2* alleviating ALI and related signaling mechanism.

developed anionic nanoparticles to deliver *pCas9-PAR2* to initiate *PAR2* deficiency by CRISPR-Cas9.

More importantly, this study revealed that PAR2 agonists could exacerbate LPS-induced acute lung inflammation, suggesting the participation of PAR2 activation (Fig. 5). To enhance drug targeting in inflamed sites, the collagen-binding peptide (CBP) was also grafted to HSA-based nanoparticles since massive collagen accumulated in inflamed tissues[19]. TAP/*pCas9-PAR2* with CBP exhibited the highest inflamed lung-targeting efficiency compared to *pCas9-PAR2* and AP/*pCas9-PAR2* (Fig. 5B, C, and Figs. S7 and S8). Surprisingly, HSA-based nanoparticles without CBP (AP/*pCas9-PAR2*) also showed relatively high fluorescence of *pCas9-PAR2* in lung, probably because it has been reported that supramolecular arrangement of proteins, such as HSA, in a nanoparticle structure can promote lung accumulation in ALI mouse, preferably triggering anti-inflammatory responses[4]. However, it is still not clear about the mechanism of inflamed lung-targeting capacity and anti-inflammatory effects of the HSA nanoparticle itself, which requires further explorations. Additionally, TAP/*pCas9-PAR2* largely prolonged the half-time and enhanced peak plasma concentration of *pCas9-PAR2*, endowing its excellent bioavailability for potent gene editing of *PAR2* (Fig. 3A, Table S5). With elevated pharmacokinetic properties, TAP/*pCas9-PAR2* robustly promoted *PAR2* knockout by CRISPR-Cas9 to alleviate lung inflammation of ALI mouse, playing a protective role in inflamed lungs (Fig. 5). By contrast, it has been reported that PAR2-mediated cAMP accumulation activated by thrombin acutely prevented TLR4-dependent Ca^{2+} signalling and inflammation in alveolar macrophages[36]. It is probably because there are the Yin−Yang roles of PAR2, pro-inflammatory and anti-inflammatory effects that are context-dependent (cell type, ligands and the environment[9]. Moreover, *PAR2* deficiency by TAP/*pCas9-PAR2* powerfully mitigated various proinflammatory cytokine secretions, including IL-6, TNF-α, IL-1β, in lungs with low short-term toxicity, revealing that it is conducive to preventing the deterioration of cytokines storm and lung inflammation (Fig. 6, Fig. S12).

Alternatively, we further explored the underlying mechanism of TAP/*pCas9*-PAR2-inhibited lung inflammation (Fig. 4). *PAR2* deficiency by TAP/*pCas9-PAR2* initiated transformation of M1 to M2 anti-inflammatory macrophages and suppressed abundant cytokine expressions in inflammatory cells (Figs. 4A and B, L, and 6A−C). Importantly, we uncovered the active involvement of NLRP3 inflammasome signalling, since TAP/*pCas9-PAR2* remarkably prevented PAR2-induced NLRP3 inflammasome, and subsequently alleviated its downstream Caspase-1 and IL-1β secretion in both inflammatory cells and ALI mouse (Figs. 4 and 6C−D). Although NLRP3 inflammasome as a cytoplasmic community signaling complex drastically participates in the pathogenesis of inflammatory diseases[37] and its activation can be modulated through some GPCRs, such as GRP40/120, MT1/2, EP4 and TGR5[38], there is a lack of studies on PAR2 and NLRP3 signal cascade. Indeed, our findings provided a novel direction for elucidating PAR2-mediated inflammation. It has been reported that ERK/2 signnalling was a classical PAR2-mediated pathway[39], and also participated in NLRP3 inflammasome activation[40]. Consistently, TAP/*pCas9-PAR2* dramatically suppressed PAR2-induced classical ERK1/2 signalling pathway (Fig. 4C, D, I, and J), suggesting the participation of ERK-mediated NLRP3/Caspase-1/IL-1β signalling. Additionally, *PAR2* knockout by TAP/*pCas9-PAR2* largely mitigated another inflammatory signalling, NO/iNOS pathway, through inhibiting PAR2-induced iNOS and NO productions (Fig. 4G, H, and Fig. S6). There are also emerging evidence that NLRP3 inflammasome and iNOS signalling cooperatively modulated various inflammatory responses[41], supporting our results of ERK/NLRP3 inflammasome and NO/iNOS pathways involved in PAR2-mediated inflamm-ation.

5. Conclusions

This study constructed a novel anionic nanoparticle to encapsulate *pCas9-PAR2*, exhibiting superior stability and pharmacokinetic

properties. TAP/*pCas9-PAR2* remarkably elevated cell uptake and transfection efficiency of *pCas9-PAR2*, consequently evoking *PAR2* deficiency *in vivo* and *in vivo*. Interestingly, we revealed a novel proinflammatory role of PAR2 in ALI, and TAP/*pCas9-PAR2* initiated precise *PAR2* knockout to suppress PAR2-induced ALI *via* ERK/NLRP3/Caspase-1/IL-1β signalling and NO/iNOS pathways (Fig. 7). Therefore, we firstly developed CRISPR-Cas9-based nanoparticles for gene editing of *PAR2* as a gene therapy strategy with extraordinary anti-inflammatory effects in ALI, providing a novel value of *PAR2* deficiency and underlying signalling mechanism for treating inflammatory diseases.

Acknowledgments

This work was supported by the National Natural Science Foundation of China (Nos. 82003784 and 81872789), the Fundamental Research Funds for the Central Universities (No. 2682022ZTPY037, China), Large Instruments Open Foundation of Southwest Jiaotong University (No. 2022SRII-046, China). We also thank Ruiping Huai for primer design in evaluation of gene editing efficiency. We greatly thank Gerui Fan for valuable suggestions and discussions.

Author contributions

Yuhong Jiang designed the research. Yuhong Jiang, Xin Zhuo, Yue Wu and Xiujun Fu carried out the experiments and performed data analysis. Jianbin Li, Yuxin Xiang, Xiaoyu Liang participated part of the experiments. Xin Zhuo drafted the manuscript and Yuhong Jiang edited the manuscript. Yuhong Jiang and Canquan Mao revised the manuscript. All of the authors have read and approved the final manuscript.

Conflicts of interest

The authors have no conflicts of interest to declare.

Appendix A. Supporting information

Supporting data to this article can be found online at https://doi.org/10.1016/j.apsb.2023.08.013.

References

1. Feehan KT, Gilroy DW. Is resolution the end of inflammation?. *Trends Mol Med* 2019;**25**:198−214.
2. Gangoda L, Schenk RL, Best SA, Nedeva C, Louis C, D'Silva DB, et al. Absence of pro-survival A1 has no impact on inflammatory cell survival *in vivo* during acute lung inflammation and peritonitis. *Cell Death Differ* 2022;**29**:96−104.
3. Jiang K, Yang J, Guo S, Zhao G, Wu H, Deng G. Peripheral circulating exosome-mediated delivery of miR-155 as a novel mechanism for acute lung inflammation. *Mol Ther* 2019;**27**:1758−71.
4. Myerson JW, Patel PN, Rubey KM, Zamora ME, Zaleski MH, Habibi N, et al. Supramolecular arrangement of protein in nanoparticle structures predicts nanoparticle tropism for neutrophils in acute lung inflammation. *Nat Nanotechnol* 2022;**17**:86−97.
5. Cao X. COVID-19: immunopathology and its implications for therapy. *Nat Rev Immunol* 2020;**20**:269−70.
6. Tay MZ, Poh CM, Rénia L, MacAry PA, Ng LFP. The trinity of COVID-19: immunity, inflammation and intervention. *Nat Rev Immunol* 2020;**20**:363−74.
7. Jimenez-Vargas NN, Pattison LA, Zhao P, Lieu T, Latorre R, Jensen DD, et al. Protease-activated receptor-2 in endosomes signals persistent pain of irritable bowel syndrome. *Proc Natl Acad Sci USA* 2018;**115**:7438−47.
8. Steinhoff M, Vergnolle N, Young S, Tognetto M, Amadesi S, Ennes H, et al. Agonists of proteinase-activated receptor 2 induce inflammation by a neurogenic mechanism. *Nat Med* 2000;**6**:151−8.
9. Zhuo X, Wu Y, Fu X, Liang X, Xiang Y, Li J, et al. The Yin−Yang roles of protease-activated receptors in inflammatory signalling and diseases. *FEBS J* 2022;**289**:4000−20.
10. Jiang Y, Yau M-K, Lim J, Wu KC, Suen JY, Fairlie DP. A potent antagonist of protease-activated receptor 2 that inhibits multiple signaling functions in human cancer cells. *J Phamacol Exp Ther* 2018;**364**:246−57.
11. Ran FA, Hsu PD, Wright J, Agarwala V, Scott DA, Zhang F. Genome engineering using the CRISPR-Cas9 system. *Nat Protoc* 2013;**8**:2281−308.
12. Li L, Hu S, Chen X. Non-viral delivery systems for CRISPR/Cas9-based genome editing: challenges and opportunities. *Biomaterials* 2018;**171**:207−18.
13. Zhang X, Jin H, Huang X, Chaurasiya B, Dong D, Shanley TP, et al. Robust genome editing in adult vascular endothelium by nanoparticle delivery of CRISPR-Cas9 plasmid DNA. *Cell Rep* 2022;**38**:110196.
14. Wang P, Zhang L, Xie Y, Wang N, Tang R, Zheng W, et al. Genome editing for cancer therapy: delivery of Cas9 Protein/sgRNA plasmid *via* a gold nanocluster/lipid core-shell nanocarrier. *Adv Sci* 2017;**4**:1700175.
15. Wei T, Cheng Q, Min YL, Olson EN, Siegwart DJ. Systemic nanoparticle delivery of CRISPR-Cas9 ribonucleoproteins for effective tissue specific genome editing. *Nat Commun* 2020;**11**:3232.
16. Blanco E, Shen H, Ferrari M. Principles of nanoparticle design for overcoming biological barriers to drug delivery. *Nat Biotechnol* 2015;**33**:941−51.
17. Rhaese S, von Briesen H, Rübsamen-Waigmann H, Kreuter J, Langer K. Human serum albumin-polyethylenimine nanoparticles for gene delivery. *J Control Release* 2003;**92**:199−208.
18. Huang D, Chen YS, Green CR, Rupenthal ID. Hyaluronic acid coated albumin nanoparticles for targeted peptide delivery in the treatment of retinal ischaemia. *Biomaterials* 2018;**168**:10−23.
19. Katsumata K, Ishihara J, Mansurov A, Ishihara A, Raczy MM, Yuba E, et al. Targeting inflammatory sites through collagen affinity enhances the therapeutic efficacy of anti-inflammatory antibodies. *Sci Adv* 2019;**5**:1971.
20. Du XJ, Wang JL, Iqbal S, Li HJ, Cao ZT, Wang YC, et al. The effect of surface charge on oral absorption of polymeric nanoparticles. *Biomater Sci* 2018;**6**:642−50.
21. Look J, Wilhelm N, von Briesen H, Noske N, Günther C, Langer K, et al. Ligand-modified human serum albumin nanoparticles for enhanced gene delivery. *Mol Pharm* 2015;**12**:3202−13.
22. Kimura K, Yamasaki K, Nakamura H, Haratake M, Taguchi K, Otagiri M. Preparation and *in vitro* analysis of human serum albumin nanoparticles loaded with anthracycline derivatives. *Chem Pharm Bull* 2018;**66**:382−90.
23. Langer K, Balthasar S, Vogel V, Dinauer N, Von Briesen H, Schubert D. Optimization of the preparation process for human serum albumin (HSA) nanoparticles. *Int J Pharm* 2003;**257**:169−80.
24. Sevigny LM, Zhang P, Bohm A, Lazarides K, Perides G, Covic L, et al. Interdicting protease-activated receptor-2-driven inflammation with cell-penetrating pepducins. *Proc Natl Acad Sci U S A* 2011;**108**:8491−6.
25. Suen JY, Cotterell A, Lohman RJ, Lim J, Han A, Yau MK, et al. Pathway-selective antagonism of proteinase activated receptor 2. *Br J Pharmacol* 2014;**171**:4112−24.
26. Lawrence T, Natoli G. Transcriptional regulation of macrophage polarization: enabling diversity with identity. *Nat Rev Immunol* 2011;**11**:750−61.

27. Youm YH, Nguyen KY, Grant RW, Goldberg EL, Bodogai M, Kim D, et al. The ketone metabolite β-hydroxybutyrate blocks NLRP3 inflammasome-mediated inflammatory disease. *Nat Med* 2015;**21**:263−9.
28. Kayagaki N, Warming S, Lamkanfi M, Walle LV, Louie S, Dong J, et al. Non-canonical inflammasome activation targets caspase-11. *Nature* 2011;**479**:117−21.
29. Hutchings CJ, Koglin M, Olson WC, Marshall FH. Opportunities for therapeutic antibodies directed at G-protein-coupled receptors. *Nat Rev Drug Discov* 2017;**16**:787−810.
30. Blázquez-Prieto J, López-Alonso I, Huidobro C, Albaiceta GM. The emerging role of neutrophils in repair after acute lung injury. *Am J Respir Cell Mol Biol* 2018;**59**:289−94.
31. Dunbar CE, High KA, Joung JK, Kohn DB, Ozawa K, Sadelain M. Gene therapy comes of age. *Science* 2018;**359**:6372.
32. Zhao M, Wang R, Yang K, Jiang Y, Peng Y, Li Y, et al. Nucleic acid nanoassembly-enhanced RNA therapeutics and diagnosis. *Acta Pharm Sin B* 2022;**13**:916−41.
33. Chen Z, Liu F, Chen Y, Liu J, Wang X, Chen AT, et al. Targeted delivery of CRISPR/Cas9-mediated cancer gene therapy *via* liposome-templated hydrogel nanoparticles. *Adv Funct Mater* 2017;**27**:1703046.
34. Li H, Wang Y, Tang Q, Yin D, Tang C, He E, et al. The protein corona and its effects on nanoparticle-based drug delivery systems. *Acta Biomater* 2021;**129**:57−72.
35. Huang B, Tan Z, Bohinc K, Zhang S. Interaction between nanoparticles and charged phospholipid membranes. *Phys Chem Chem Phys* 2018;**20**:29249−63.
36. Rayees S, Joshi JC, Tauseef M, Anwar M, Baweja S, Rochford I, et al. PAR2-mediated cAMP generation suppresses TRPV4-dependent Ca^{2+} signaling in alveolar macrophages to resolve TLR4-induced inflammation. *Cell Rep* 2019;**27**:793−805.
37. Mangan MSJ, Olhava EJ, Roush WR, Seidel HM, Glick GD, Latz E. Targeting the NLRP3 inflammasome in inflammatory diseases. *Nat Rev Drug Discov* 2018;**17**:588−606.
38. Tang T, Gong T, Jiang W, Zhou R. GPCRs in NLRP3 inflammasome activation, regulation, and therapeutics. *Trends Pharmacol Sci* 2018;**39**:798−811.
39. Jiang Y, Lim J, Wu KC, Xu W, Suen JY, Fairlie DP. PAR2 induces ovarian cancer cell motility by merging three signalling pathways to transactivate EGFR. *Br J Pharmacol* 2021;**178**:913−32.
40. Chei S, Oh HJ, Song JH, Seo YJ, Lee K, Kim KJ, et al. Spirulina maxima extract prevents activation of the NLRP3 inflammasome by inhibiting ERK signaling. *Sci Rep* 2020;**10**:1−10.
41. Jiang M, Wang H, Liu Z, Lin L, Wang L, Xie M, et al. Endoplasmic reticulum stress-dependent activation of iNOS/NO-NF-κB signaling and NLRP3 inflammasome contributes to endothelial inflammation and apoptosis associated with microgravity. *Faseb J* 2020;**34**:10835−49.